Ion dynamics in a highly compressed solution of tetra-ethylammonium – tetra-fluoroborate salt in propylene carbonate: A study in the equilibrium and glassy states

Marco Bonetti

▶ **To cite this version:**

Marco Bonetti. Ion dynamics in a highly compressed solution of tetra-ethylammonium – tetra-fluoroborate salt in propylene carbonate: A study in the equilibrium and glassy states. Journal of Non-Crystalline Solids, 2022, 595, pp.121831. ⟨10.1016/j.jnoncrysol.2022.121831⟩. ⟨hal-04335433⟩

HAL Id: hal-04335433

https://hal.science/hal-04335433v1

Submitted on 14 Dec 2023

HAL is a multi-disciplinary open access archive for the deposit and dissemination of scientific research documents, whether they are published or not. The documents may come from teaching and research institutions in France or abroad, or from public or private research centers.

L'archive ouverte pluridisciplinaire **HAL**, est destinée au dépôt et à la diffusion de documents scientifiques de niveau recherche, publiés ou non, émanant des établissements d'enseignement et de recherche français ou étrangers, des laboratoires publics ou privés.

HAL Authorization

Ion dynamics in a highly compressed solution of tetra-ethylammonium – tetra-fluoroborate salt in propylene carbonate: a study in the equilibrium and glassy states

Marco Bonetti

Université Paris-Saclay

CEA, CNRS, SPEC

Service de Physique de l'Etat Condensé

F-91191 Gif sur Yvette

France

Abstract: Electrical conductivity of a solution of (Et_4N^+, BF_4^-) in propylene carbonate is measured by varying the pressure and temperature along different thermodynamic paths: pressure is increased from a low value in the liquid state up to ~ 3.6 GPa well above the glass-transition pressure P_G, along isotherms at temperatures between ~ 295 K and ~ 326 K. Up to a crossover pressure P_{cross} ~ 1 GPa, the *dc*-conductivity decreases and obeys the Walden rule. Above P_{cross}, an anomalous pressure-dependence of the conductivity spectra is observed, leading to an increase in *dc*-conductivity up to P_G. The *dc*-conductivity obeys density scaling, showing in the glassy state an exponential decrease against the scaling variable, independently of the thermobaric history of the sample. The conductivity spectra obey the *time-temperature-pressure-superposition* principle, therefore, the ion dynamics is not affected by the transition from the liquid state to the non-ergodic glassy state.

1. Introduction

Understanding the transport properties of tracers (molecules, ions, ...) in supercooled liquids and glassy materials has many important applications[1-3] ranging from drug delivery through amorphous polymer matrices,[4] charge transport in solid-state batteries,[5,6] chemical hazard where, *e.g.*, the diffusion of radio-active elements through the vitreous matrix must be controlled for nuclear waste immobilization.[7-9] In this regard, during the last decades, considerable attention has been paid to the dynamics of ions in conductive disordered solids, ion-conductive glasses and conductive polymers.[10-12] More recently, the dynamics of supercooled ionic liquids has been the subject of in-depth studies.[13-20]

Knowledge of ion transport properties in glasses under extreme conditions such as high hydrostatic pressures also has technological implicance, *e.g.*, in the development of glasses with tailored properties after densification,[9,21-25] and is of great interest in the geological community to understand the geochemical process of the earth's mantle.[26-29] Indeed, studying the pressure dependence of ionic mobility provides insight into the microscopic mechanisms of ion diffusion, revealing an activated hopping mechanism in single-cation glasses[30] or an ion-coupling process in mixed-cation glasses,[31] and an ion-matrix coupling in conductive polymer glasses.[32]

The response to an electric field of mobile ions embedded in a host liquid informs about the coupling between charge carriers and the structural dynamics of the glass forming liquid.[33] This coupling depends on the interaction between the structural rearrangement of the host matrix characterized by the α-relaxation time τ_α, and the conductivity dynamics, with a relaxation time τ_σ .[34,35] In the equilibrium state, as the glassy state is approached, decoupling is observed in several ionic liquids.[13,36-38] Under these conditions, the conductivity relaxation time τ_σ and the α-relaxation time τ_α become distinguishable. The ratio τ_α/τ_σ − known as the decoupling index R − quantifies the strength of decoupling between the two relaxing modes.[10,39-41] At the glass-transition temperature T_G, the decoupling index for ionic glasses may reach values as high as ~10^{14}.[10,41] Decoupling depends on the bonding between the ions and the host liquid, and on the activation volume of the ions.[42] Small ions with relatively weak bonding usually decouple from the host matrix.

The decoupling of ion dynamics from the structural relaxation of the host matrix can lead to highly conductive systems with the aim of obtaining, *e.g.*, highly conductive solid polymer electrolytes where ion diffusion decouples from the segmental dynamics of the polymer chain structure,[43,44] or protic superionic conductors.[45] On the contrary, decoupling in glassy materials must be minimized to control the confinement of ions (or molecules) within the matrix.[46]

Some aprotic ionic liquids containing large organic ions do not exhibit decoupling of conductivity from structural dynamics[47] or a pronounced dynamic crossover of the transport properties.[48] High pressure reduces the decoupling between anionic mobility and structural relaxation in polymerized ionic liquids.[49] In contrast, decoupling is observed in protic ionic liquids under high pressures,[45,50,51] where the enhancement in proton transport is attributed to

a proton hopping mechanism along the hydrogen bond network squeezed by the high pressures. Under these conditions, protic ionic liquids exhibit a superionic conductivity.

The aim of this work is to measure the mobility of ions in a sample under high pressure for thermodynamic state points below and above the glass transition line. In this paper, the interaction of the ions with the structural heterogeneities of the host liquid[52] is investigated. Further, one questions on how the transport of ions is affected by the transition from the equilibrium liquid state to the non-ergodic glassy state. Indeed, presently, the underlying mechanism for describing charge mobility in frozen matrices and how the onset of glass non-ergodicity disrupts ion-matrix coupling is not completely understood. To answer this, we carried out conductivity measurements from a dilute solution of tetra-ethylammonium – tetra-fluoroborate salt (Et_4N^+, BF_4^-) in propylene carbonate (PC), by isothermal compression along 3 isotherms between ~ 295 K and ~ 326 K. Pressure is gradually increased from a low value in the liquid state, to about 3.6 GPa, a value higher than the glass transition pressure P_G. Complementary measurements by varying the temperature along 2 isobars in the glassy state were also made. Propylene carbonate is a well-documented liquid, which exhibits a low tendency to crystallization up to very high pressures.[53] Ion sizes comparable to PC molecules, low ionic charge, and near-perfect slip with respect to PC molecules[54] could promote the decoupling between ion mobility and structural dynamics of PC. The response of the mobile ions is measured by impedance spectroscopy in the frequency interval [0.1 – 10^5] Hz.

The present measurements evidence in the equilibrium liquid state a temperature-dependent crossover pressure P_{cross} below which the *dc*-conductivity obeys the Walden rule indicating that the ion transport couples to the structural relaxation of the host liquid. Above this crossover pressure, we observe an anomalous pressure dependence of the conductivity spectra leading to an increase of the *dc*-conductivity for increasing pressure up to P_G. In this pressure interval, and for state points located in the glassy state, we show that the real part of the conductivity spectra obeys the *time-temperature-pressure-superposition* principle (TTPS).[55] That indicates that the dynamics of mobile ions on short-length scale is independent of pressure and temperature, and is not affected by the transition from the liquid to the glassy state. We also show that the *dc*-conductivity, in the equilibrium and glassy regimes, verifies *density scaling*[55] when plotted against the scaling variable $\left(\frac{\rho^\gamma}{T}\right)$ with ρ, the density of the host fluid and γ, the scaling exponent. Density scaling evidences the observed anomalous increase of the *dc*-conductivity for state points located in the equilibrium state. In the glassy state, the *dc*-conductivity measured along isotherms and isobars collapses to a decreasing exponential function, independently of the thermobaric history of the sample. The exponential decrease is consistent with the behavior of ion-conductive glasses when cooled below T_G at constant pressure.[5,8,10,41,56,57]

We show that the anomalous increase in *dc*-conductivity occurs at approximately the same crossover pressure P_{cross} at which a dynamic change in the diffusivity of uncharged fluorescent molecules in propylene carbonate is observed. Indeed, for $P \geq P_{cross}$, from the time-recovery of the fluorescent intensity in photobleaching experiments,[58,59] the molecular diffusivity has been shown to exhibit a more Arrhenius-like behavior for increasing pressure.

This dynamic change could be related to the anomalous behavior of the ion transport observed between P_{cross} and P_G.

In Sec. 2, we describe into details the conductivity setup implemented in the DAC cell for high pressure electric conductivity measurements. In Sec. 3, we focus on conductivity measurements carried out in the equilibrium liquid state along the isotherms at $T \cong 295$ K and $T \cong 326$ K for pressures up to the crossover pressures P_{cross} ~ 1.3 GPa and ~ 1.8 GPa, respectively. Next, we focus on the anomalous conductivity spectra measured along the 326 K isotherm for increasing pressures between P_{cross} and the glass transition pressure P_G = 2.82 GPa, as well as on the spectra measured in the glassy state by varying the temperature along the ~ 3.6 GPa isobar. Section 4 deals with the analysis of the conductivity spectra measured in the equilibrium and glassy states, according to the density scaling approach and TTPS principle.

2. Experimental

2.1 High-pressure conductivity cell

High hydrostatic pressures are obtained by means of a diamond anvil cell (DAC).[60,61] The large diamond anvil culets used in our setup give a limiting pressure of ~ 6 GPa at room temperature.[58,59] This limiting pressure is well above the glass transition pressure of propylene carbonate.

The electrode wires are embedded in a composite gasket[62-64] to prevent any short-circuit with the metallic parts of the gasket sandwiched between the two anvils. The two opposite electrodes 200 μm apart are located flush with the walls of a cylindrical cavity made of insulating material. The main challenge for accurate conductivity measurement is to control the radial creeping of the composite gasket when squeezed by the anvils. With a stable gasket under compression, electrode displacement and variation of the cell constant are minimized. Here, we briefly detail the main steps to assemble a composite gasket with the two embedded electrodes. A 200 μm thick Cu-Be gasket is preindented and a groove ~ 100 μm deep and ~ 50 μm wide is machined along the diameter of the gasket. A 400 μm hole is then center-drilled by electroerosion. The hole and the deburred groove are filled with an insulating pasty mixture of Stycast epoxy 1266 and TiO_2 powder (0.3 μm averaged grain size) with a mass ratio ~ 2:1 (powder:epoxy). Then, a 50 μm diameter Manganin wire is embedded into the groove and slightly strained. To obtain a uniform thickness of the pasty mixture a sheet of mica is pressed evenly against the epoxy on each side of the gasket. Next, the epoxy paste is cured at 70°C for about 1h30. A second low-pressure indentation enables to center-drill the 200 μm diameter hole forming the sample chamber. The mica sheets prevent any chipping of the cured epoxy when the hole is drilled. In this step, the embedded Manganin wire is cut to form the two opposite electrodes flush with the cell wall. A composite gasket with the two electrodes is shown in Fig.1 where, for clarity, pure transparent Stycat epoxy has been used to help visualize the position of the embedded electrodes. Note that the composite gasket with pure epoxy insulation can withstand pressures as high as ~ 2.1 GPa at room temperature, but

in most cases the sample chamber suffers from uneven deformation leading to an unstable hole. Radial cracks in the epoxy were also observed propagating outward from the inner walls. Therefore, composite gaskets made with pure epoxy were no longer used in the present work.

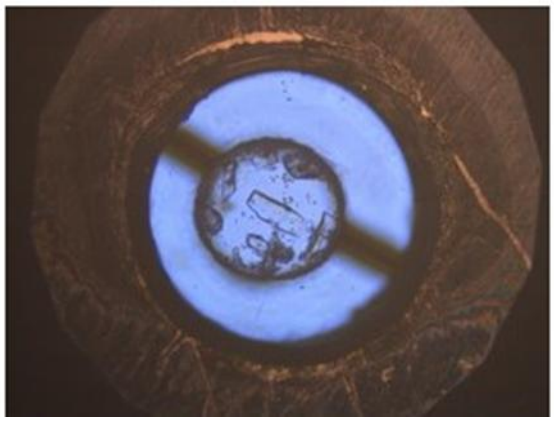

Fig. 1 Back-illuminated composite gasket. The central bright area is the 200 μm diameter sample chamber surrounded by insulating transparent epoxy Stycast. Transparent epoxy is used here to visualize the radial position of the two embedded 50 μm diameter wires with the ends flush with the cell wall. The Cu-Be gasket with a 400 μm hole appears as the brown circular area. Note the ruby chips used as a pressure gauge and placed at the bottom of the sample chamber. These crystals do not interfere with the electrical conductivity measurements. The sample pressure is ~ 2.03 GPa at room temperature.

From capacitive measurements carried out at atmospheric pressure, first with an empty unloaded cell, and then with the emptied cell previously pressurized to ~ 2.2 GPa with propylene carbonate, the increase of the cell constant attributed to the weak radial displacement of the electrodes is estimated to be less than ~ 10%. This value gives an upper bound for the uncertainty of the measured electrical conductivity.

Pressure is increased by steps of a few hundreds of MPa by means of an inflating elastic membrane which moves the diamond anvils against each other. The pressure in the sample chamber is determined by the ruby fluorescence method.[58,65] Ruby chips with 0.5 wt% Cr_2O_3, of several tens of microns, are deposited at the bottom of the chamber (see Fig. 2). During a complete pressure run, the excitation laser beam is focused at the same position on a single ruby crystal, and the fluorescence intensity is collected backwards in the spectrometer with 0.02 nm resolution which gives a pressure accuracy of ± 50 MPa. The frequency shift of the fluorescence peak R1 at wavelength λ_1 is measured as a function of the gasket compression. Pressure in the sample is determined from the pressure derivative $\frac{d\lambda_1}{dP}$ = 0.37 nm GPa^{-1} at room temperature.[65] The temperature effect is taken into account from the temperature derivative $\frac{d\lambda_1(P_{atm})}{dT}$ = 6.60×10^{-3} nm K^{-1} determined from the temperature shift of the peak R1 at atmospheric pressure. The cell temperature is controlled between ~ 283 K and ~ 338 K by means of a temperature-regulated copper block surrounding the DAC cell, giving a temperature stability of ± 0.05 K. Temperatures below ~ 283 K were not investigated due water condensation on the cell walls, while temperatures above ~ 338 K were not reached due to uneven deformation and a loss of stability of the composite gasket.

Impedance was measured in the frequency range 10^{-1} Hz - 10^5 Hz by the *I-V* method where the unknown complex impedance $Z^*(\omega)$ of the sample is obtained from the voltage drop $v(\omega)$ across a known resistance R_0 (10^5 Ω) under an applied voltage $V(\omega)$, ω being the angular frequency:

$$Z^*(\omega) = \left(\frac{V}{v} - 1\right) R_0 \qquad (1)$$

The voltage drop amplitude $|v|$ and phase angle θ are measured as a function of frequency by a lock-in amplifier (LI5640-NF, Japan) triggered by a voltage source (SRI-360, USA). The voltage drop v is corrected from the cable capacitance and the input impedance of the lock-in amplifier. Frequencies below 10^{-1} Hz were not explored as the signal is noisy, whereas frequencies higher than ~10^6 Hz would require the use of a coaxial line reflectometer with an electrodes configuration not compatible with the geometry of the DAC cell.

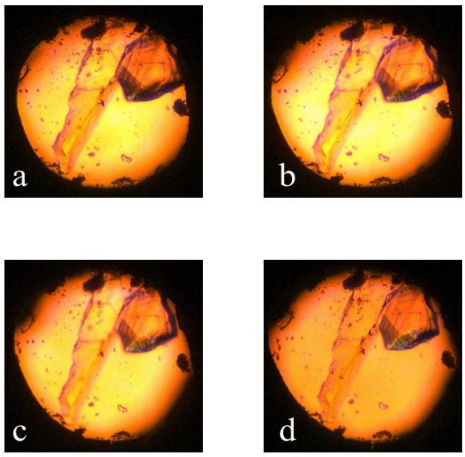

Fig.2 Microscopic views of the sample at various pressures during compression, corresponding to the electrical conductivity measurements shown in Figs. 6 and 9-b: a) 1.45 GPa, b) 1.94 GPa, c) 2.31 GPa, and d) 2.92 GPa. The diameter of the sample chamber drilled in the composite gasket is ~ 200 μm. Note the relatively large ruby crystals used as pressure gauge (see text). T = 325.80 K. The glass-transition pressure is P_G = 2.82 GPa. Solution of 10^{-2} M (Et_4N^+, BF_4^-) in propylene carbonate.

2.2 Ionic solution and phase diagram

Tetra-ethylammonium – tetra-fluoroborate salt (Et_4N^+, BF_4^-) (Sigma-Aldrich) is dissolved with a molar concentration c = 10^{-2} M in 99.7 % pure propylene carbonate (Sigma-Aldrich). Et_4N^+ cation and BF_4^- anion have a symmetrically shaped structure with van der Waals radii of respectively ~ 0.336 nm[54] and ~ (0.228 ± 0.001) nm.[54,66] These radii compare to the calculated PC radius ~ 0.276 nm.[54] Et_4N^+ and BF_4^- ions exhibit rather perfect slip with respect to PC molecules.[54] This suggests that the ion mobility is mostly sensitive to the structural heterogeneities and the relaxation dynamics of PC. Propylene carbonate has a glass

transition temperature T_G ~160 K[67] at atmospheric pressure It is a good glass former with a low tendency to crystallize at high pressure.[53] In the pressure range [0 – ~4] GPa, dielectric spectra of pure PC are composed mainly from the structural α-relaxation and no secondary β-relaxation is observed.[53,68] PC has a large dielectric permittivity ε = 66 at 298 K and a large dipole moment ~ 4.9 D that impedes ion association (ion pairs or higher ion aggregates) in the mixture.[69,70] As shown in Sec. 3, a concentration of 10^{-1} M does not modify the shape of the dielectric loss spectra in an extended pressure range. We therefore focused on conductivity measurements carried out with a solution at 10^{-2} M.

The glass transition pressure P_G of the 10^{-2} M solution is determined from the method based on the enlargement of the width $\Delta\lambda$ (nm) at half-maximum (FWHM) of the peak R_1 from the fluorescent emission of the ruby crystal embedded in the sample under pressure.[59,65] When the sample under uniaxial compression approaches the glass transition, stress gradients settle in the sample due to the high value of the sample viscosity.[65] These non-hydrostatic stresses lead to a broadening of the peak R_1 at wavelength λ_1. Therefore, the value of the wavelength λ_1 and the enlargement of the peak R_1 depend on the position of the focused laser beam in the sample. The pressure distribution in the sample can be evidenced by placing tiny ruby chips at different locations in the cell.[71] In the present case, due to the relatively large size of the ruby crystals (see Fig. 2), the broadening of the peak R1 results from the spatial average of non-hydrostatic stresses surrounding the ruby crystal, and the pressure is a spatially-averaged value over the ruby crystal dimensions.

Figure 3 shows the variation of the width $\Delta\lambda$ as a function of pressure in a solution 10^{-2} M (Et_4N^+, BF_4^-) in PC at T = 295.35 K and 326.10 K. Pressure is increased by steps of few hundreds of MPa with a pressurizing rate $\frac{dP}{dt}$ between ~3 MPa.s^{-1} and ~5 MPa.s^{-1}. The pressure corresponding to the onset of the line broadening - shown by a vertical arrow - defines the glass transition pressure P_G. For the isotherms at T = 295.35 K, 312.25 K and 326.10 K we find P_G ~ 2.30 ± 0.05 GPa, 2.70 ± 0.05 GPa ($\Delta\lambda$ variation not shown in Fig.3)) and 2.82 ± 0.05 GPa, respectively.

The value P_G = 2.30 GPa for the isotherm at T = 295.35 K is close to the glass transition pressure P_G = 2.12 GPa calculated from the dielectric measurements of Kondrin *et al.*[53] in pure PC at T = 292.3 K, corresponding to the isochronal line τ_α ~ 150 s. The current glass-transition pressure is also very close to P_G ~ 2.29 GPa measured in a solution of 10^{-3} M Coumarin 1 in PC at 296 K using the ruby fluorescence method.[59] This shows that the weak ion concentration in the solution does not modify – within the ± 50 MPa pressure accuracy – the glass transition pressure.

In the temperature and pressure ranges studied, microscopic observation did not reveal any phase transformation that would indicate crystallization of the sample. The sample always appeared homogeneously transparent as shown in Fig. 2 for pressure larger than P_G. Even for pressures as high as P ~ 6 GPa reached in Fig. 4 along the isotherm at T = 326.1 K, no crystallization was observed. Indeed, the monotonic increase of $\Delta\lambda$ for pressures higher than P_G does not indicate any structural change in the solution that would be induced by the compression.[72]

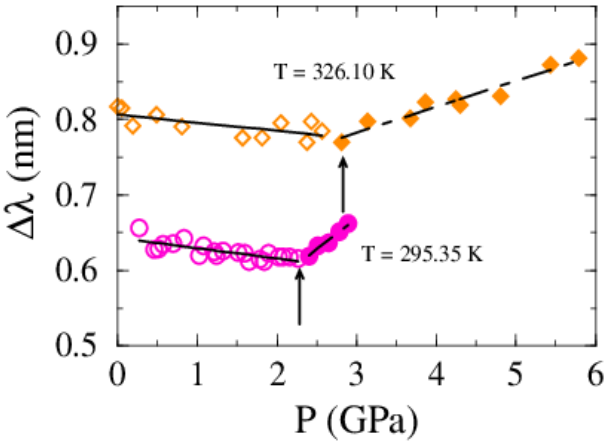

Fig. 3 Width $\Delta\lambda$ at half maximum (FWHM) of the peak R1 as a function of pressure, from the fluorescence emission of a ruby crystal embedded in a solution of 10^{-2} M (Et_4N^+, BF_4^-) in propylene carbonate. Fluorescence is measured by increasing the pressure from the atmospheric pressure along isotherms at T = 295.35 K (circles), and T = 326.10 K (diamonds). The lines are linear regressions for data points belonging to the liquid state (open symbols), or to the glassy state (filled symbols). The position of the vertical arrows located at the intersection of two regression lines defines the glass-transition pressure P_G. Measurements at T = 295.35 K are obtained with a composite gasket, whereas measurements at T = 326.10 K are made with a Cu-Be gasket to cover a larger pressure range.

The phase diagram of the solution 10^{-2} M (Et_4N^+, BF_4^-) in propylene carbonate is shown in Fig. 4. The current glass-transition (P_G-T_G)-state points determined from the ruby fluorescence method detailed previously, are represented by filled diamonds.

On the same figure we show the liquid-glass transition line (dashed line) of pure PC defined as the locus of (P-T)-state points for which the structural relaxation time τ_α ~ 150 s. In the pressure interval studied, the transition line is well described by a linear regression passing through the state points (open circles) obtained from the high-pressure dielectric spectroscopy measurements carried out by Kondrin *et al.*[53] in pure PC. It can be noticed that the glass-transition state points reported for the ionic solution and for the pure PC, obtained from two different techniques do indeed collapse on the same liquid-glass transition line.

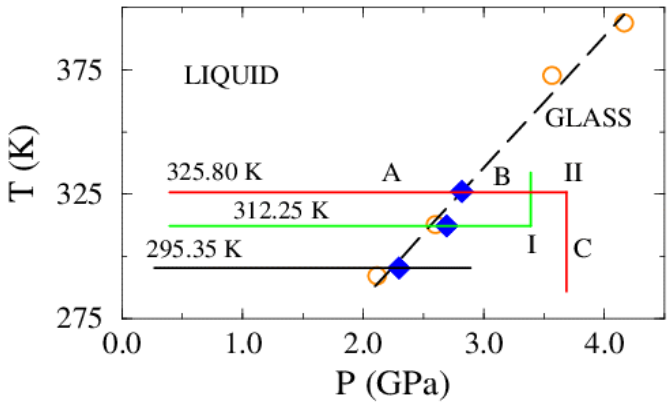

Fig.4 Phase diagram of the solution 10^{-2} M (Et_4N^+, BF_4^-) in propylene carbonate. Blue filled diamonds: current measured glass-transition (P_G-T_G)-state points obtained by the ruby fluorescence method. Dashed line: τ_α ~ 150 s isochronal line of pure PC obtained from high-pressure dielectric spectroscopy measurements (orange open circles) by Kondrin *et al.*[53] The solid thick lines show the (*P*-*T*) paths along which the electrical conductivity is measured (see text). Note that to initially seal the sample volume, the gasket must first be slightly squeezed by the anvils. The measurements therefore do not start at atmospheric pressure.

3. Results

Electrical conductivity of a solution 10^{-2} M (Et_4N^+, BF_4^-) in PC was measured along 3 routes spanning the (*P*-*T*) phase diagram as shown by the thick lines in Fig. 4. Pressure is increased along isotherms at *T* = 295.35 K, 312.25 K and 325.80 K that begin in the liquid state and intersect the liquid-glass transition line represented by the dashed line. The isotherms studied terminate in the glassy state well above the glass-transition pressure P_G. At the end point of the isotherms at *T* = 312.25 K and 325.80 K, the temperature is varied at constant pressure: at point I, the temperature is increased from 312.25 K to 333.75 K along the isobar at *P* = 3.31 GPa; at point II, the temperature is lowered from 325.80 K to 286.22 K along the isobar at *P* = 3.63 GPa (see Fig.4).

To characterize the charge transport in ion conductive systems the complex admittance formalism is used:

$$Y^*(\omega) = \frac{1}{Z^*(\omega)} = K^{-1}\,\sigma^* = j\omega\varepsilon_0\varepsilon^*\,K^{-1} \quad (1)$$

where $Y^*(\omega) = Y' + jY''$ is the complex admittance and $\omega = 2\pi f$ is the angular frequency of the applied electric field. $\sigma^*(\omega) = \sigma' + j\sigma''$ is the complex electric conductivity of the sample and $\varepsilon^*(\omega) = \varepsilon' - j\varepsilon''$ is the complex permittivity related to the bulk polarization induced by the orientation of mobile ions[73] and PC molecules. ε_0 is the vacuum permittivity and *K* (m^{-1}) stands for the cell constant. From Eq. (1) the complex conductivity is related to the complex permittivity by $\sigma^*(\omega) = j\omega\varepsilon_0\varepsilon^*(\omega)$, hence, the real part of the electrical conductivity is $\sigma'(\omega) = \omega\varepsilon_0\epsilon''(\omega)$ and the imaginary part is $\sigma''(\omega) = \omega\varepsilon_0\epsilon'(\omega)$. That shows that σ^* and ε^* share the same information and that conduction and polarization in ion conductive materials are closely related. In our analysis we will focus on the complex spectra $\sigma^*(\omega)$ and $\varepsilon^*(\omega)$ and omit the approach based on the electric modulus $M^*(\omega) = \frac{1}{\varepsilon^*(\omega)} = \frac{j\omega\varepsilon_0}{\sigma^*(\omega)}$ formalism.[74,75]

3.1 Equilibrium liquid state

Low-pressure range: The complex electric conductivity spectra ($\sigma'(\omega), \sigma''(\omega)$) for the solution 10^{-2} M (Et_4N^+, BF_4^-) in PC is shown in Fig.5 for increasing pressures between 0.27 GPa and 1.32 GPa along the isotherm at *T* = 295.35 K, and in Fig. 6 between 0.40 GPa and 1.75 GPa along the isotherm at *T* = 325.80 K. The spectra for the isotherm at *T* = 312.25 K

have similar shape and are not shown. The low-pressure ranges studied are well below the glass transition pressure P_G = 2.30 GPa and 2.82 GPa for the 295.35 K and 325.80 K isotherms, respectively. Note that the P_G value is the same within the ± 50 MPa accuracy for the 325.8 K and 326.1 K isotherms.

Overall, the general trend of the pressure-dependent spectra is similar to that observed in ionic liquids or conductive glass-forming liquids when the temperature is lowered towards the glass transition temperature.[13-20,35] The real part $\sigma'(\omega)$ of the complex electrical conductivity is shown in Figs.5-a and 6-a. For each pressure investigated, a slightly frequency-dependent plateau (or near-plateau) is observed, which corresponds to the *dc*-conductivity regime. In this frequency region, long-range ion diffusion takes place. The *dc*-plateau is not perfectly flat certainly due to the polarization of the electrodes.[76,77] For increasing pressures, the position of the near-plateau moves to the low frequencies and the corresponding *dc*-conductivity value decreases.

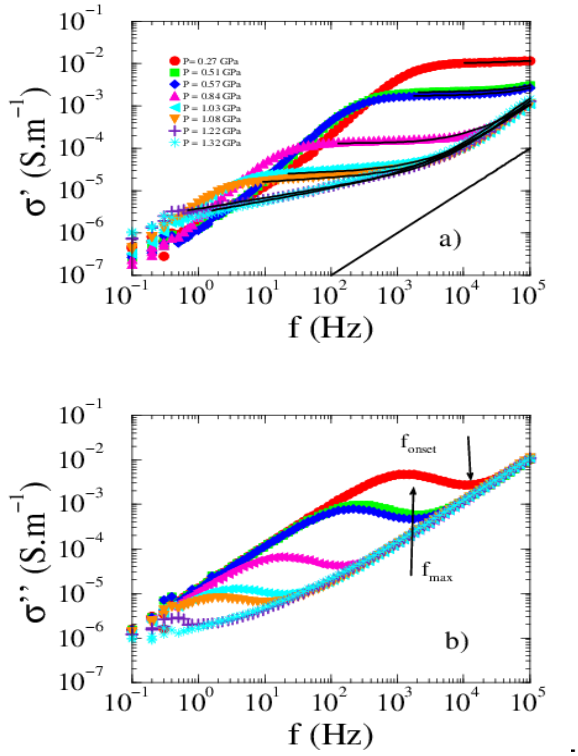

Fig. 5 Equilibrium liquid state: Electrical conductivity spectra (σ', σ'') for increasing pressures along the isotherm at T = 295.35 K. In a), the solid lines are a fit to Eq. (3), see text. In b), f_{onset} represents the frequency at the onset of electrode polarization, and f_{max} is the frequency below which full electrode polarization takes place. Pressure from top to bottom spectra: 0.27, 0.51, 0.57, 0.84, 1.03, 1.08, 1.22 and 1.32GPa. Solution of 10^{-2} M (Et_4N^+, BF_4^-) in propylene carbonate.

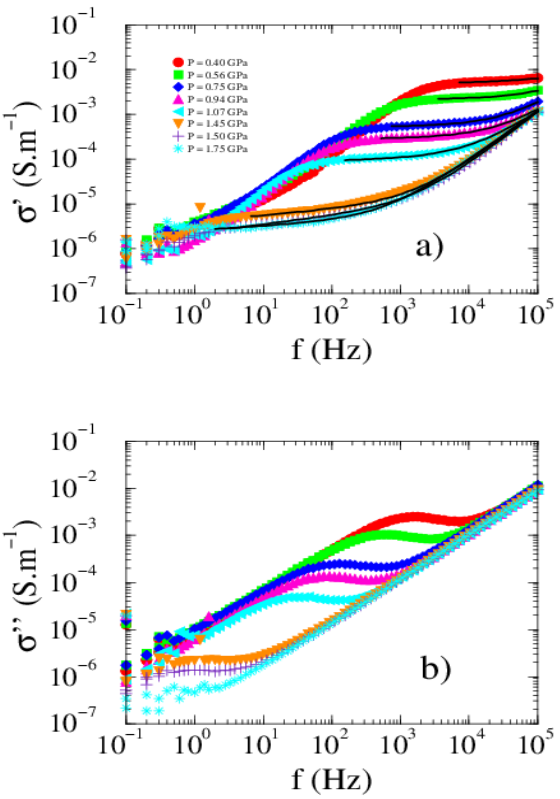

Fig. 6 Equilibrium liquid state: Same as Fig. 5 but for the isotherm at T = 325.80 K. Pressure from top to bottom spectra: 0.40, 0.56, 0.75, 0.94, 1.07, 1.45, 1.50 and 1.75 GPa.

Electrode polarization is responsible for the strong decrease of $\sigma'(\omega)$ at low frequency. At low pressures, the electrode polarization spans over a frequency interval that extends towards the high frequencies because the ion polarization at the blocking electrodes and the ion mobility within the electric double layer are favored by the low viscosity of propylene carbonate. High pressures lead to an increase of viscosity and a decrease of the ion mobility. That shifts to the low frequencies the interface dynamics. Even though the electrode polarization can be modeled by a constant phase impedance,[78-80] in our analysis we will omit the frequency interval where the electrode polarization takes place.

Within the frequency interval studied, for pressures greater than ~ 0.4 GPa, the *dc*-conductivity plateau crosses over to a frequency-dependent conductivity. This regime known as the dispersive regime is described well by a frequency power-law. The crossover region between long-range diffusive to dispersive regimes corresponds to the "Universal Dynamics Response" (UDR) regime.[81-83] For pressures above ~1 GPa, the power-law exponent is close to unity as shown in Fig. 5-a by the full line.

The effect of the electrode polarization shows up in the imaginary part $\sigma''(\omega)$ in Figs. 5-b and 6-b. A broad peak and a local minimum in $\sigma''(\omega)$ are observed at each pressure. According to Serghei *et al.*[84], the minimum at frequency f_{onset} is attributed to the onset of the electrode polarization, and the peak at f_{max} corresponds to the full polarization of the ions at the electrodes on a time scale $\tau \sim 1/2\pi f_{max}$. For increasing pressures, the peaks at f_{max} shift to the low frequencies in agreement with the frequency shift of the *dc*-conductivity plateau.

The calculated dielectric spectra $(\varepsilon', \varepsilon'')$ for increasing pressure along the isotherm at T = 295.35K are shown in Fig. 7. At low frequencies, the permittivity spectra $\varepsilon'(\omega) = \frac{\sigma''(\omega)}{\omega\varepsilon_0}$ exhibit an increase mainly caused by the capacitance of the double layer resulting from the polarization of the ions at the electrode/electrolyte interface. It should be noted that the increase of $\varepsilon'(\omega)$ is much weaker than in pure ionic liquids and their mixtures[18,19,85,86] where a variation by more than ~ 5 orders of magnitude has been observed. The dielectric loss spectra $\varepsilon''(\omega) = \frac{\sigma'(\omega)}{\omega\varepsilon_0}$ are shown in Fig. 7-b. A broad peak that moves to the low frequencies for increasing pressures characterizes the spectra. It is attributed to the relaxation loss of orientationally mobile ions within the electric double layer.[85] The high frequency flank of the peak decreases as ω^{-1} and extends over a frequency interval corresponding to the plateau in the $\sigma'(\omega)$ spectrum. For pressures greater than ~1 GPa, a weak bump in the $\varepsilon''(\omega)$ spectra is noticed at frequencies around 10^5 Hz. It is the signature of a structural relaxation process, the tail of the frequency peak of which becomes visible when the relaxation frequency approaches the frequency window studied. This secondary loss peak can be attributed to the structural relaxation of polar propylene carbonate molecules.

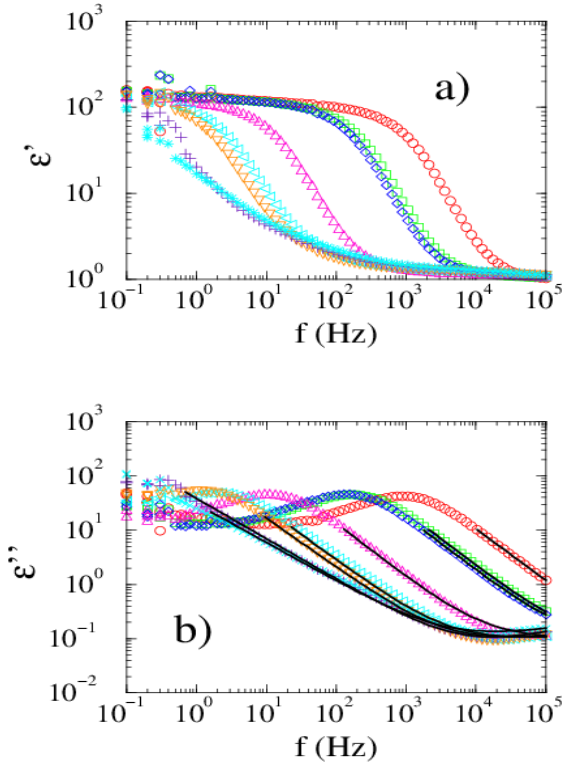

Fig. 7 Equilibrium liquid state: Dielectric spectra $(\varepsilon', \varepsilon'')$ for increasing pressures along the isotherm at T = 295.35 K. The dielectric spectra are calculated from the conductivity spectra (σ', σ'') shown in Fig. 5. Pressure from right to left: 0.27, 0.51, 0.57, 0.84, 1.03, 1.08, 1.22 and 1.32 GPa. In b), the frequency interval where ε'' varies as f^{-1} corresponds to the frequency range where a *dc*-conductivity plateau is observed in the σ'spectra. Solid lines are the calculated dielectric loss from the fit of σ' to Eq. (3) shown in Fig. 5-a. Solution of 10^{-2} M (Et_4N^+, BF_4^-) in propylene carbonate.

The effect of a higher salt concentration c = 10^{-1} M on the loss spectra $\varepsilon''(\omega)$ is shown in Fig. 8 for pressures between atmospheric pressure and ~ 1.22 GPa. A higher salt concentration shifts the spectra $\varepsilon''(\omega)$ towards high frequencies while maintaining the same spectral shape. In the frequency window studied, this reduces the frequency interval where the decrease in ω^{-1} is observed, thus it narrows the frequency range of the *dc*-conductivity plateau. We therefore focused in this work on measurements with a sample at a concentration of 10^{-2} M.

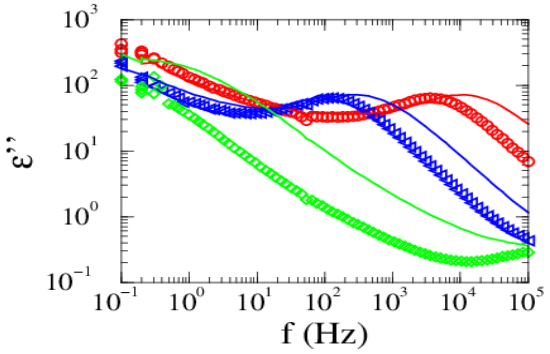

Fig.8 Equilibrium liquid state: Dielectric loss spectra $\varepsilon''(\omega)$ of a solution of (Et_4N^+, BF_4^-) in propylene carbonate with a molar concentration 10^{-2} M (symbols) and 10^{-1} M (lines), measured at three pressures. Symbols from right to left: atmospheric pressure, 0.51 GPa and 1.22 GPa. T = 295.4 K.

High-pressure range approaching P_G:

The reported conductivity spectra were measured after an equilibration time varying from a few hours to about a few days to stabilize the composite gasket and achieve a stable sample pressure. The constant value of the pressure was verified by measuring any shift of the peak R1 before and after each recording of conductivity spectra.

In the liquid state below the glass-transition line, the stabilization time is always larger than the Maxwell relaxation time $\tau \sim {}^{\eta}/_{G_\infty}$ of the stresses induced in the sample after a pressure increment. Here, η is the shear viscosity of the sample and G_∞ is the infinite frequency shear modulus. A rough estimate of τ for propylene carbonate at the liquid-glass transition, with $\eta \sim 10^{12}$ Pa.s (a typical value at the glass-transition), and $G_\infty \sim$ 2.7 GPa estimated at T = 296 K and $P = P_G$ ~ 2.3 GPa,[59] gives $\tau \sim 10^3$ s. Consequently, conductivity measurements in the liquid state are always carried out at equilibrium since the equilibration time greatly exceeds τ.

Under these stable experimental conditions, reproducible measurements of the conductivity were obtained. In this range of high pressures and in the frequency interval studied, the spectra $\sigma'(\omega)$ show a different trend compared to the measurements at low-pressure presented previously in Figs. 5 and 6. Indeed, by increasing the pressure above a temperature-dependent crossover pressure P_{cross}, the spectra show an anomalous pressure dependence. The spectra now display a well-defined plateau with a *dc*-conductivity value that increases with increasing

pressure. Figure 9-a shows how the spectra (labelled by lines) settle to a shape exhibiting a *dc*-conductivity plateau after a stabilization time of ~ 22 h following a pressure rise from ~ 1.72 GPa to ~2.01 GPa along the isotherm at T = 312.25 K. Note that in this time interval, the width $\Delta\lambda$ of the peak R1 of the ruby fluorescence emission remains constant, indicating that no crystallization-induced shear stresses occur in the sample.

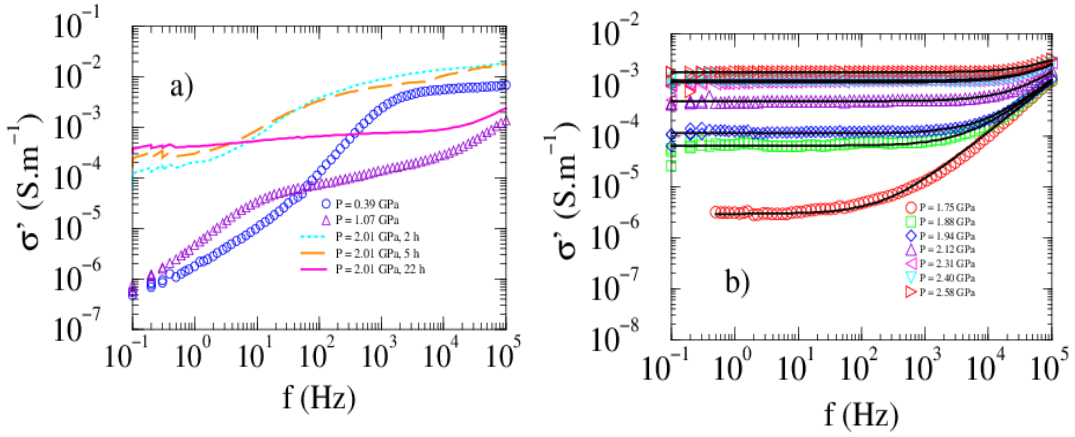

Fig. 9 Equilibrium liquid state. a) Time equilibration of the conductivity spectra σ′(ω) (labelled by lines) after a pressure rise from 1.72 GPa to 2.01 GPa along the isotherm at T = 312.25 K: stabilization time of 2 h, 5 h and 22 h. b) Spectra σ′(ω) measured along the isotherm at T = 325.80 K for increasing pressures between 1.75 GPa and 2.58 GPa. The glass-transition pressure is P_G = 2.82 GPa. Pressure from bottom to top spectra: 1.75, 1.88, 1.94, 2.12, 2.31, 2.40 and 2.58 GPa. Solid lines are fits to Eq. (2), see text. Solution of 10^{-2} M (Et_4N^+, BF_4^-) in propylene carbonate.

In Fig. 9-b, we present the conductivity spectra $\sigma'(\omega)$ measured along the isotherm at T = 325.80 K for increasing pressure between the crossover pressure P_{cross} ~1.8 ± 0.1 GPa and ~ 2.58 GPa (path A, Fig. 4). This latter pressure is close to the glass-transition pressure P_G ~ 2.82 GPa. The spectra are characterized by a well-defined *dc*-conductivity plateau that shifts upwards with increasing pressure. In this pressure range, the electrode polarization effect is not visible, presumably because it takes place at low frequencies outside the frequency window studied. This is due to the large value of the viscosity at these pressures.

This anomalous trend is also observed for the isotherm at T = 312.25 K. For the 295.35 K isotherm, an upward shift of the spectra for increasing pressure above P_{cross} ~1.3 ± 0.1 GPa is observed but no well-defined plateau was noticed.

3.2 Glassy state

The crossing of the glass-transition line is achieved with a pressurization rate $\frac{dP}{dt}$ similar to that used for the determination of the glass-transition (P_G-T_G)-state points discussed in Sec. 2.2, *i.e.*, $\frac{dP}{dt}$ is comprised between ~ 3 MPa.s^{-1} and ~5 MPa.s^{-1}

In the glassy state by increasing pressure between P_G and ~3.31 GPa along the isotherm at T = 325.8 K (path B, Fig. 4), the $\sigma'(\omega)$ spectra (not shown) have a well-defined *dc*-conductivity plateau with a *dc*-conductivity value that slightly decreases.

Figure 10 shows the σ′(ω) spectra for decreasing temperature from 325.80 K (point II, Fig.4) to 286.22 K along the isobar at P = 3.63 GPa (path C, Fig. 4). The spectra have a similar shape characterized by a *dc*-conductivity plateau with a conductivity value that undergoes a pronounced decrease when the temperature is lowered. Conversely, the temperature increase from 312.25 K (point I, Fig.4) to 333.75 K for the isobar at P = 3.31 GPa shows spectra of similar shape with increasing values of *dc*-conductivity (spectra not shown). These variations of *dc*-conductivity as a function of temperature show that the spectra are indeed related to the temperature-dependent dynamics of the ions in the glassy state. This is best evidenced when analyzing the data in terms of density scaling.

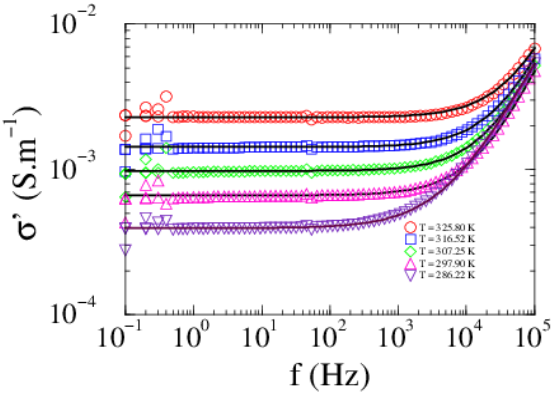

Fig.10 Glassy state: Electrical conductivity spectra σ′(ω) for decreasing temperatures from 325.80 K to 286.22 K along the isobar at P = 3.63 GPa (path C, Fig. 4). Solid lines are fits to Eq. (2). Solution of 10^{-2} M (Et_4N^+, BF_4^-) in propylene carbonate.

4. Analysis of the admittance spectra and discussion

For amorphous materials such as ion conducting glasses or crystalline solids the real part σ′(ω) of the electrical conductivity is characterized by a *dc*-conductive term and a frequency-dependent dispersive term at frequencies below a few tens of MHz. The spectra $\sigma'(\omega)$ can be described by the empirical Jonscher power-law:[11,76,77,81,87]

$$\sigma'(\omega) = \sigma_0 \left(1 + \left(\frac{\omega}{\omega_{on}}\right)^n\right), \qquad (2)$$

where σ_0 is the bulk *dc*-conductivity corresponding to the plateau in $\sigma'(\omega)$, $\omega_{on} = 2\,\pi\, f_{on}$ is the onset angular frequency at which dispersion occurs, and n is an exponent between 0 and 1. The Jonscher power-law associates the onset of the dispersive conductivity in disordered systems with the hopping of correlated charge carriers. The onset frequency ω_{on} can be interpreted as the hopping rate of charge carriers in the matrix,[11] or as the characteristic relaxation frequency of space charge fluctuations.[87] Note that for $\omega = \omega_{on}$, $\sigma'_s = 2\sigma_0$. Eq. (2) is observed in the frequency interval where the effect of the electrode polarization can be

neglected, *i.e.*, for frequencies higher than the onset frequency f_{onset} corresponding to the local minimum in the $\sigma''(\omega)$ spectrum (see Fig. 5-b).

According to Almond *et al.*[88], the slightly frequency-dependent *dc*-conductivity plateau observed in Figs. 5 and 6 for the isotherms at T = 295.35 K and 325.80 K could result from additional dispersion due to ions moving bodily at low frequencies. This mechanism can be modeled by introducing a second Jonscher power-law. However, the fit with two Jonscher power-laws proved to be very unstable with a poor determination of the fitting parameters, and was not used further in our analysis. Nowick *et al.*[76] has estimated the *dc*-conductivity by extrapolating the slightly frequency-dependent plateau to a low frequency. In the present case, the near-plateau is fitted to a power-law $\sigma(\omega_0)\,(\frac{\omega}{\omega_0})^b$ where the exponent b is a fitting parameter ranging from 0.05 to 0.23. We define the *dc*-conductivity $\sigma_0 = \sigma(\omega_0)$ as the value of the power-law extrapolated to the low frequency f_0 = 0.1 Hz. The fits to Eq. (3):

$$\sigma'(\omega) = \sigma(\omega_0)\,(\frac{\omega}{\omega_0})^b \left(1 + \left(\frac{\omega}{\omega_{on}}\right)^n\right) \qquad (3)$$

are shown as full lines in Figs. 5-a and 6-a. The *dc*-conductivity $\sigma_0 = \sigma(\omega_0)$ plotted against pressure for the isotherm at T = 295.35 K is represented by filled circles in Fig. 11 where a decrease by ~ 4 orders of magnitude is observed in the pressure range [0 - ~1.25] GPa. Note that the *dc*-conductivity in the high-pressure range P > ~ 1.25 GPa is not shown due to undetectable *dc*-plateaus within the frequency window studied.

A pressure-dependent Vogel-Fulcher-Tammann (VFT) function[42,89] exp(-a $P/(P_0\text{-}P)$) fits well the conductivity data for the 295.35 K isotherm with the fitted parameters a = 4.942 and P_0 = 2.67 GPa. In the same figure, we show as filled squares the fluidity ($1/\eta$) of pure PC at T = 298.15 K from high-pressure shear viscosity measurements by Casalini and Bair.[90] The fluidity data are fitted to a pressure-dependent VFT function as shown by the full line in Fig. 11.

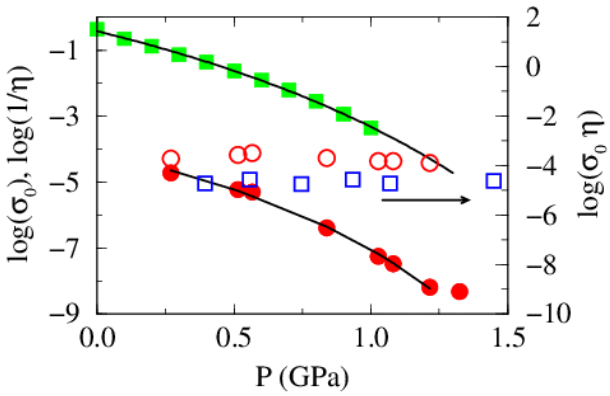

Fig. 11 Pressure-dependent *dc*-conductivity σ_0 (S.m^{-1}) along the isotherm at T = 295.35 K (filled circles), fluidity $1/\eta$ (mPa^{-1}.s^{-1}) of pure propylene carbonate at T = 298.15 K from the measurements by Casalini and Bair[90] (filled squares), and Walden product ($\sigma_0\,\eta$) along the isotherms at T = 295.35 K (open circles) and T = 325.80 K (open squares). Full lines are fits to pressure-dependent VFT functions (see text). To calculate the Walden product at pressures greater than ~ 1 GPa, extrapolated values of the fluidity $1/\eta$ are obtained from the VFT function. Solution of 10^{-2} M (Et_4N^+, BF_4^-) in propylene carbonate.

The Walden product[91] $(\sigma_0\,\eta)$ is displayed as a function of pressure in Fig. 11 for the isotherms at T = 295.35 K (open circles) and T = 325.80 K (open squares), where we use the high-pressure viscosity measurements of Casalini and Bair[90] obtained at slightly higher temperatures 298.15 K and 328.15 K. The nearly constant value of $(\sigma_0\,\eta)$ for both isotherms indicates that the ion transport couples to structural relaxation of the host liquid via viscosity dependence. The constant value of the Walden product also indicates that the interaction between ions does not change in this temperature-pressure range.[92]

Conductivity measurements made in the near vicinity of the liquid-glass transition line and in the glassy state show well-defined *dc*-conductivity plateaus in $\sigma'(\omega)$. This is well evidenced for the two runs starting in the liquid state along the isotherms at T = 312.25 K and 325.80 K. The spectra fitted to Eq. (2) from measurements made along the isotherm at T = 325.80 K (paths A, Fig. 4)), and along the isobar at P = 3.31 GPa (path C, Fig. 4) are represented by solid lines in Figs.9-b and 10.

The values of the fitted parameters σ_0 and ω_{on} of Eq. (2) are shown as a function of pressure in Fig. 12 from measurements performed along the 325.80 K isotherm in the liquid and glassy states. In the liquid state between ~ 1.75 GPa and ~2.58 GPa, σ_0 and ω_{on} show a pronounced increase by ~3-orders of magnitude against pressure and the two curves have similar shape. In the vicinity of P_G, σ_0 and ω_{on} remain finite. At the glass transition, we observe a rise in σ_0, and an exponential decrease of σ_0 and ω_{on} against pressure could be guessed in the glassy state. The exponential decrease is best evidenced when analyzing the *dc*-conductivity in term of the density scaling approach, exploiting additional conductivity measurements made along isobars and isotherms in the glassy state.

Although the anomalous increase of σ_0 observed above the crossover pressure is not strictly speaking a decoupling between charge transport and structural dynamics,[17] an estimate of the decoupling index $R = {}^{\tau_\alpha}/_{\tau_\sigma}$ at the glass transition gives R ~ 10^{10}. Here, $\tau_\sigma \sim \left(\frac{\varepsilon_0\varepsilon_\infty}{\sigma_0}\right)$ is the relaxation time of the *dc*-conductivity,[34,35] and $\tau_\alpha \sim 150\ s$ is the structural relaxation time at the glass transition. The estimated *R*-value is much higher than the value found in other ionic liquids,[37,38] although decoupling indices as high as ~ 10^{14} have been recorded in some ionic glasses.[10]

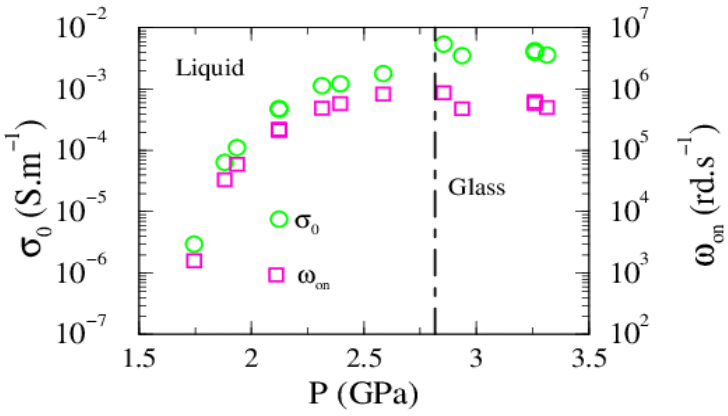

Fig. 12 Variation of *dc*-conductivity σ_0 and dispersive frequency ω_{on} for increasing pressure, from a fit to Eq. (2) of the $\sigma'(\omega)$ spectra measured along the isotherm at T = 325.80 K. The vertical dashed line indicates the glass-transition pressure P_G = 2.82 GPa. Solution of 10^{-2} M (Et_4N^+, BF_4^-) in propylene carbonate.

Figure 12 shows in a double-logarithm plot the *dc*-conductivity σ_0 as a function of the dielectric relaxation $\varepsilon_0 \Delta\varepsilon\, \omega_{on}$ for the liquid state (path A, Fig. 4), and for the glassy state (paths B and C, Fig. 4). $\Delta\varepsilon = (\varepsilon_s - \varepsilon_\infty)$ is the dielectric strength of the bulk mixture which takes into account the permittivity due the relaxation of the mobile ions and the polar molecules of PC. ε_s is the static permittivity and ε_∞ the permittivity at infinite frequency. The data either for the liquid state or for the glassy state collapse well onto two distinct lines of unit slope within the (*P*-*T*) phase diagram studied. Note that in these plots, we have set $\Delta\varepsilon = \Delta\varepsilon_{PC} \sim 60$ as the dielectric strength $\Delta\varepsilon_{PC}$ of PC is found to be constant between atmospheric pressure and ~ 4 GPa.[53] The linear correlation between the two quantities is similar to the empirical Barton-Nakajima-Namikawa (BNN) relationship $\sigma_0 = p\varepsilon_0 \Delta\varepsilon\, \omega_{on}$ observed in a large number of conducting glasses,[11, 48,93,94] where the correlation parameter p is of order 1. From a fit to the BNN relation, the correlation factor in the liquid state is p ~ 4, and p ~ 12 in the glassy state. The increase in p by a factor ~ 3 at P_G can be attributed to a step increase in dielectric strength $\Delta\varepsilon$ associated with the collection of ions.

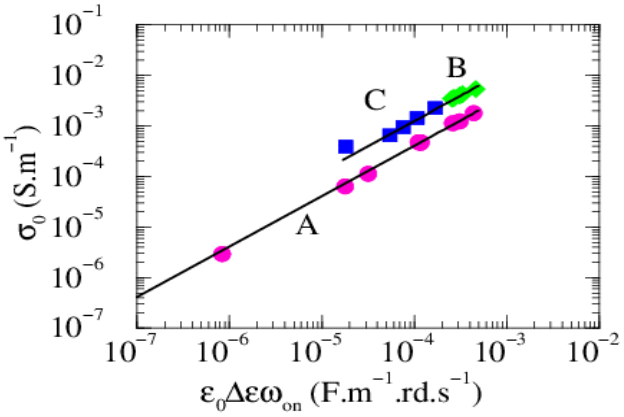

Fig. 13 Log-log plot of the *dc*-conductivity σ_0 as a function of the dielectric relaxation $\varepsilon_0 \Delta\varepsilon\, \omega_{on}$. Liquid state, path A: pressure increase from 1.75 GPa to 2.58 GPa along the isotherm at T = 325.80 K (circles). Glassy state: path B, pressure increase between 2.85 GPa and 3.63 GPa along the isotherm at T = 325.80 K (diamonds); path C, temperature decrease from 325.80 K to 286.22 K along the isobar at P = 3.63 GPa (squares). The solid lines with unit slope are fits to the BNN relation, see text. Solution of 10^{-2} M (Et_4N^+, BF_4^-) in propylene carbonate.

Combining the Nernst-Einstein equation with the BNN relation,[12,95] one obtains for the expression of the dielectric strength $\Delta\varepsilon$:

$$\epsilon_0 \Delta\varepsilon = \frac{N q^2 \zeta^2}{6\, kT}\ , \qquad (4)$$

where N is the number density of mobile ions, q the ion charge, and ζ the mean hopping length. Therefore, the increase in $\Delta\varepsilon$ at P_G is related to a change of $N\zeta^2$across the glass transition, *i.e.*, a change in ion concentration and/or hopping length. As we show in the next paragraph, the ion dynamics obeys the time-temperature-pressure superposition principle (TTPS) in either the liquid state or the glassy state. This indicates that the dynamics of the

ions remains unchanged across the liquid-glass transition line,[12] so the hopping length ζ should be constant. Therefore, the change in $\Delta\varepsilon$ must be attributed to a change in the number density N of mobile ions at the transition line which results in an increase in *dc*-conductivity. Note that an increase in $\Delta\varepsilon$ is observed in some ion-conducting glasses when crossing the glass transition *upon* heating. It is attributed to a change in the population of mobile ions present in the sample.[12,95]

TTPS principle: Equation (2) suggests that scaling $\sigma'(\omega)$ by the *dc*-conductivity σ_0 and the angular frequency by the onset dispersive frequency ω_{on} would generate a master curve.[55,96-98] The master curve reflects the nature of ion transport on short-length scales, independent of the thermodynamic state point. The scaled conductivity is shown in Fig. 14 for measurements made in the liquid and glassy states along paths A, B and C shown in Fig.4. All the curves overlap on a single curve. The plateau for scaled frequencies $(\frac{\omega}{\omega_{on}})$ between ~10^{-6} and ~10^{-1} corresponds to the *dc*-conductivity regime, while for scaled frequencies $\left(\frac{\omega}{\omega_{on}}\right) \geq 1$ dispersion begins. Figure 14 clearly shows that a *time-pressure superposition* holds for increasing pressures in the equilibrium state below P_G (path A), and in the glassy state well above P_G (path B). Similarly, the decrease in temperature in the glassy state along the isobar at P = 3.63 GPa (path C) shows that a *time-temperature superposition* is obeyed. Stated in other words, the shape of the scaled conductivity spectra is invariant in the investigated temperature-pressure domain and therefore a *time-temperature-pressure superposition* (TTPS) principle is applicable.[55] In the temperature-pressure domain studied, whether in the equilibrium state or in the glassy state, the dynamics of ions is independent of pressure and temperature, and is not affected by the liquid-glass transition. Therefore, no changes in the local environment surrounding the ions or structural changes in the solution that would perturb the dynamics of mobile ions occurs in the liquid and glassy states. This is supported by the monotonic increase of the width $\Delta\lambda$ of the ruby fluorescence line against pressure shown in Fig. 3, which indicates that no structural change occurs in the glassy state by super-pressing up to ~ 6 GPa.

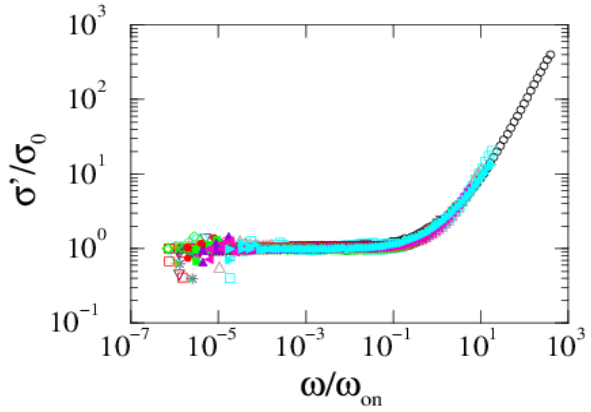

Fig.14 Log-log plot of the scaled conductivity spectra σ'/σ_0 as a function of the scaled frequency ω/ω_{on}, for increasing pressure between 1.75 GPa and 3.31 GPa along the isotherm at T = 325.80 K, and for decreasing temperature from 325.80 K to 286.22 K along the isobar at P = 3.63 GPa. Solution of 10^{-2} M (Et_4N^+, BF_4^-) in propylene carbonate.

Density scaling: Thermodynamic scaling (or density scaling) allows analysis of the relaxation time and transport properties of glass-forming liquids to be made as a function of a single scaling variable $\left(\frac{\rho^{\gamma}}{T}\right)$ where ρ is the density of the fluid and γ is a material-dependent scaling exponent.[55] The scaling exponent γ mainly depends on the steepness of the repulsive intermolecular potential[55,99] and the conformation of the molecules.[99] When the glass-forming system obeys density scaling within the (*P*-*T*) domain, the structural relaxation time collapses on a single master curve when plotted against $\left(\frac{\rho^{\gamma}}{T}\right)$.[100-102] It has been shown that for transport quantities such as viscosity, diffusivity or electrical conductivity, density scaling also applies.[99,102-104] For van der Waals liquids, γ takes on the values between ~ 3 and ~ 8 for structural relaxation time collapse,[55] whereas for viscosity or electrical conductivity of molecular liquids or ionic liquids γ varies between ~ 1.2 and ~ 13.[99,103,105] High-pressure measurements have shown that the scaling exponent could vary with temperature and density.[106,107] For non-associated low polar liquids, a limiting value $\gamma \sim 4$ is observed at elevated pressures consistent with a repulsive intermolecular potential with inverse power law exponent $n = 12$ through the relationship $\gamma = n/3$.[106,107]

Pawlus *et al.*[108] have found $\gamma = 3.7$ for the structural relaxation time and viscosity of propylene carbonate in a pressure range [0 - ~ 1.8] GPa. The same value of γ leads to a collapse of the diffusive time of fluorescent molecules in PC for measurements carried out in the pressure range [0 - ~1.7] GPa at different temperatures.[59] The low value of γ for PC might be caused by the high polarity of PC.[107] In the present analysis, we assume constant the γ value within the (*P*,*T*) range studied.

In Fig. 15 we show the *dc*-conductivity σ_0 as a function of the scaling variable $\left(\frac{\rho^{\gamma}}{T}\right)$ normalized by $\left(\frac{\rho_G^{\gamma}}{T_G}\right)$, $\gamma = 3.7$, for measurements made along the 3 routes in the liquid state up to the liquid-glass transition line.[109] This plot is equivalent to a plot of σ_0 against the scaling variable $\left(\frac{\rho^{\gamma}}{T}\right)$ because by definition of the glass transition boundary T_G (P_G), along the isochronal line the α-structural relaxation time is constant and writes $\tau_{\alpha}(P_G, T_G) \sim C \left(\frac{\rho_G^{\gamma}}{T_G}\right) \sim 150$ s.[71,101,109]

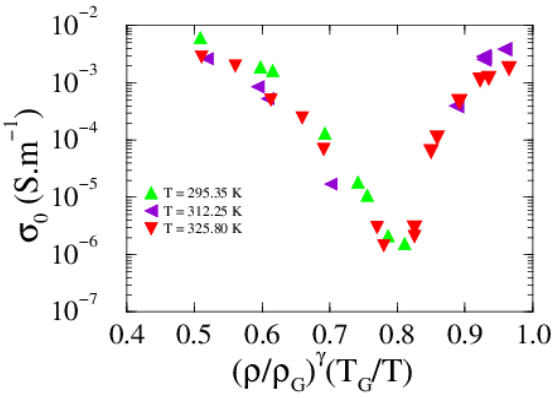

Fig. 15 Liquid equilibrium state: Variation of the *dc*-conductivity σ_0 as a function of the normalized scaling variable $\left(\frac{\rho}{\rho_G}\right)^{\gamma}\left(\frac{T_G}{T}\right)$, $\gamma = 3.7$, for measurements carried out along the 3 isotherms at T = 295.35 K, 312.25 K and 325.80 K, by increasing the pressure up to the glass-transition pressure P_G. Solution of 10^{-2} M (Et_4N^+, BF_4^-) in propylene carbonate.

Normalization by $\left(\frac{\rho_G^{\gamma}}{T_G}\right)$ was made using the experimental values of the glass-transition (P_G, T_G)-state points determined by the ruby fluorescence method. The density ρ of the solution was calculated using the modified Tait equation of state of propylene carbonate by Casalini and Roland[110] given for a pressure range [0 - ~ 1.8] GPa. In absence of *PVT* measurements at higher pressures, we assume that the modified Tait equation is valid in the (*P*-*T*) range studied. The average value of $\left(\frac{\rho_G^{\gamma}}{T_G}\right)^{-1}$, calculated between 295.35 K and 325.80 K and for glass transition pressures P_G in the range between ~ 2.30 GPa and~ 2.82 GPa, is 141 ± 6 (K.g$^{-\gamma}$.cm$^{3\gamma}$), γ = 3.7. The low dispersion in $\left(\frac{\rho_G^{\gamma}}{T_G}\right)^{-1}$ indicates that the modified Tait equation is applicable in the investigated pressure interval.

On close inspection to Fig. 15 we observe that for $\left(\frac{\rho}{\rho_G}\right)^{3.7}\left(\frac{T_G}{T}\right) \leq$ ~ 0.8 the *dc*-conductivity σ_0 decreases by about 4-orders of magnitude. In this (*P*-*T*) range, the ion dynamics is coupled to the α-relaxation dynamics of the host liquid as was shown by the constant value of the Walden product displayed in Fig. 11. The anomalous increase of σ_0 begins at the crossover pressure P_{cross} ~ 1.3 GPa and ~1.8 GPa for the isotherms at T = 295.35 K and 325.80 K, respectively. These pressures coincide to the normalized scaling variable $\left(\frac{\rho^{\gamma}}{\rho_G^{\gamma}}\frac{T_G}{T}\right)$ ~ 0.8. By further increasing the pressure until the glass transition, *i.e.*, for the normalized scaling variable between ~ 0.8 and 1, we observe an increase in σ_0 which reaches a value close to the *dc*-conductivity at low pressure.

Pawlus *et al.*[108] have shown from dielectric relaxation measurements carried out in propylene carbonate, that a dynamic crossover of the electrical conductivity takes place at a pressure P_{cross} ~ 1 GPa along the isotherm at T = 284 K. These results show that the α-relaxation time associated to the dynamic change is invariant to pressure and temperature, and is the main parameter that governs the dynamic crossover. Similarly, Bonetti and Dubois[59] showed a non-monotoneous variation against pressure of the exponent β of the Kohlrausch function (stretched exponential function) which describes well the time recovery of the fluorescent intensity of diffusive Coumarin 1 molecules in pressurized propylene carbonate. The Kohlrausch exponent β takes on values between 0 and 1, and characterizes the departure from a pure exponential relaxation ($\beta = 1$). A minimum of β occurs at P_{cross} ~ 1 ± 0.1 GPa and ~ 1.5 ± 0.2 GPa at temperature T = 296 K and 325.5 K, respectively. The subsequent increase in the stretched exponent β from ~ 0.6 to ~ 0.8 observed between P_{cross} and P ~ 0.6 × P_G, reflects a change in the time-diffusivity of the fluorescent molecules that becomes more Arrhenius-like for increasing pressure. Figure 16 outlines the almost linear variation of the crossover pressure P_{cross} as a function of temperature for the measurements herein detailed. Clearly, the diffusivity of uncharged Coumarin 1 molecules and the transport of ions (Et_4N^+, BF_4^-) in

propylene carbonate exhibit a dynamics change at approximately the same crossover pressure for a given temperature.

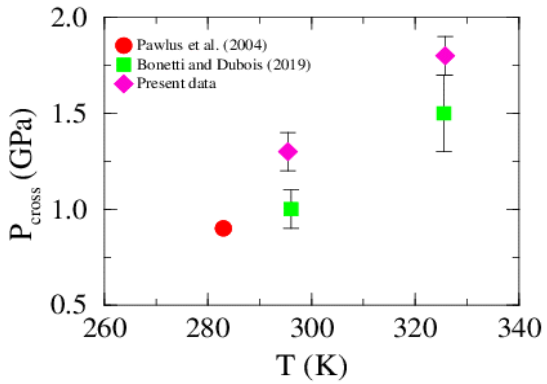

Fig. 16 Crossover pressure P_{cross} as a function of temperature, determined from: dielectric relaxation measurements carried out by Pawlus *et al.*[108] in propylene carbonate (circle), fluorescence intensity recovery after photobleaching from a solution of 10^{-3} M Coumarin 1 in propylene carbonate (squares) by Bonetti and Dubois,[59] and conductivity measurements in a solution of 10^{-2} M (Et_4N^+, BF_4^-) in propylene carbonate (diamonds), this work.

The minimum at P_{cross} of the Kohlrausch exponent β, that characterizes the diffusivity of uncharged molecules in propylene carbonate, and its increase for pressures higher than P_{cross}, could be correlated with the change in the conductivity spectra observed at P_{cross}. The increase of the *dc*-conductivity observed between P_{cross} and P_G could be related to a more Arrhenius-like transport of the charges.

In Fig. 17, the *dc*-conductivity σ_0 is shown as a function of the scaling variable $\left(\frac{\rho^\gamma}{T}\right)$, $\gamma = 3.7$, for measurements made in the glassy state at increasing pressure along the isotherms at T = 312.25 K and 325.80 K, and by varying the temperature along the isobars at P = 3.31 GPa and 3.63 GPa. It should be emphasized that we apply density scaling to measurements made in the glassy state for which the validity of density scaling is unknown.[111] It can be noted that all the measured conductivities σ_0 collapse on a single curve exhibiting a well-defined exponential decrease $\sigma_0(\rho, T) \propto \exp(-A_\sigma \frac{\rho^\gamma}{T})$.

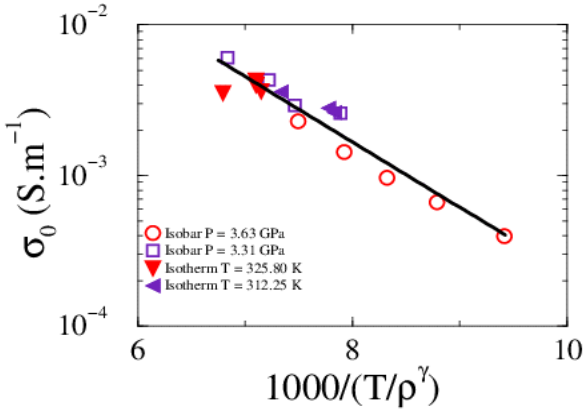

Fig. 17 Glassy state: Arrhenius plot of the *dc*-conductivity σ_0 as a function of the scaling variable $\left(\frac{\rho^\gamma}{T}\right)$, γ = 3.7. Filled symbols: pressure increase from the glass-transition line along the isotherms at T = 312.25 K and

325.80 K (see Fig. 4). Open symbols: temperature variation along the isobars at P = 3.31 GPa and 3.63 GPa. Solid line: fit to an exponential function. Solution of 10^{-2} M (Et_4N^+, BF_4^-) in propylene carbonate.

The solid line in Fig. 17 shows the exponential fit with the fitted parameter A_σ ~1000 (K.g$^{-\gamma}$.cm$^{3\gamma}$), γ = 3.7. This behavior is consistent with the Arrhenius behavior observed in ionic glasses when cooled, at constant pressure, below their glass transition temperature.[41,56,57] Note that the same value of the γ exponent is used either in the liquid and glassy states. As γ is related to the power-law exponent of the intermolecular potential, the constant value of γ indicates that the interaction between mobile ions does not change with temperature and pressure, and across the liquid-glass transition line. This is in agreement with the TTPS principle applicable either in the liquid and glassy state.

A glass being a non-ergodic system, the properties of the glass are modified by its thermobaric history. In this regard, Danilov *et al*.[23] showed that glassy PC obtained after different thermobaric quenches exhibits different elastic and shear properties. These differences in behavior are attributed to the "*closure of nanopores*" – corresponding to the medium-range order structure – in PC after a ~ 1 GPa pressure quench followed by a thermal quench into the glassy state. In the present case, changes in elastic and shear properties in the glassy state, accompanied by structural changes at medium-range, have no effect on the exponential decrease of the *dc*-conductivity observed in the glassy state whatever the thermodynamic paths.

5. Conclusion

The electric conductivity of a dilute solution of (Et_4N^+, BF_4^-) in propylene carbonate was measured by increasing the pressure along isotherms from the equilibrium liquid state to the glassy state, and inside the glassy state by varying the temperature along isobars. At low pressures in the liquid state, the *dc*-conductivity is coupled to the structural dynamics of the host liquid via the viscosity dependence. From a temperature-dependent crossover pressure of order ~1 GPa, the conductivity spectra show an anomalous behavior characterized by a well-defined *dc*-conductivity plateau that shifts upwards with increasing the pressure up to the glass-transition pressure P_G. This anomalous behavior is characterized by an increase of the *dc*-conductivity with pressure, and should not be attributed to a decoupling between ion conductivity and structural relaxation, as is commonly observed in ion conducting glass-forming liquids. In the glassy state, the measured *dc*-conductivity decreases slightly for increasing pressures along isotherms, whereas it shows a pronounced variation as temperature increases or decreases along isobars.

The anomalous behavior observed in the equilibrium state does not appear to be an experimental artifact nor the consequence of sample crystallization. This is reinforced by the fact that scaling by $\left(\frac{\rho}{\rho_G}\right)^\gamma \left(\frac{T_G}{T}\right)$, γ = 3.7, collapses the *dc*-conductivity data measured along isotherms up to the glass-transition line. In the glassy state, we show that the *dc*-conductivity exhibits an exponential decrease with respect to the scaling variable $\left(\frac{\rho^\gamma}{T}\right)$, γ = 3.7,

independently of the thermobaric history of the sample. The Arrhenius law observed in the glassy state is similar to that observed in ion conducting glasses when cooled below their glass-transition temperature.

Although the range of pressure and temperature studied is limited by experimental constraints, we have shown that the dynamics of correlated mobile ions obeys the TTPS principle both in the liquid state and the glassy state. This indicates that the ion dynamics on short-length scales is independent of temperature and density, and is unaffected by the transition from the equilibrium liquid state to the non-ergodic glassy state.

We have shown that the diffusivity of uncharged molecules and the ionic conductivity in pressurized propylene carbonate experience a change at approximately the same temperature-dependent crossover pressure. The more Arrhenius-like diffusivity of uncharged molecules for pressures larger than P_{cross} could be correlated with the increase in *dc*-conductivity observed between P_{cross} and $P_{\text{G.}}$

The underlying mechanism to explain the anomalous dynamics on large scales by increasing pressure above P_{cross} remains yet to be understood. Our results could possibly be interpreted within the framework of the bypass clusters model[10,112-114] with preferred pathways for ion migration. These pathways could have liquid-like properties that would enhance the ion transport.

Acknowledgements

V. Padilla, D. Duet, C. Gasquet-Wiertel and S. Delprat are thanked for their technical assistance.

References

1. R. Zhang and K.S. Schweizer, *J. Chem. Phys.*, 2017, **146**, 199406.
2. R.C. Roberts, R. Poling-Skutvik, J.C. Palmer and J.C. Conrad, *J. Phys. Chem. Lett.*, 2018, **9**, 3008.
3. R.C. Roberts, R. Poling-Skutvik, J.C. Conrad and J.C. Palmer, *J. Chem. Phys.*, 2019, **151**, 194501.
4. S. Baghel, H. Cathcart and N.J. O'Reilly, *J. Pharm. Sci.*, 2016, **105**, 2527.
5. M. Tatsumisago and A. Hayashi, *Solid State Ionics*, 2012, **225**, 342.
6. R.C. Xu, X.H. Xia, Z.J. Yao, X.L. Wang, C.D. Gu and J.P. Tu, *Electrochim. Acta*, 2016, **219**, 235.
7. B.J. Riley, J. D. Vienna, D.M. Strachan, J.S. McCloy and J.L. Jerden Jr, *J. Nucl. Mat.*, 2016, **470**, 307.
8. B.K. Maji, H. Jena and R. Asuvathraman, *J. Non-Cryst. Solids*, 2016, **434**, 102.
9. V. Jolivet, Y. Morizet, J. Hamon, M. Paris and T. Suzuki-Muresan, *J. Am. Ceram. Soc.*, 2021, **104**, 1360.
10. C. A. Angell, *Chem. Rev.*, 1990, **90**, 523.
11. J. C. Dyre, P. Maass, B. Roling and D. L. Sidebottom, *Rep. Prog. Phys.*, 2009, **72**, 046501.
12. D.L. Sidebottom, *Rev. Mod. Phys.*, 2009, **81**, 999.
13. A. Rivera, A. Brodin, A. Pugachev and E.A. Rössler, *J. Chem. Phys.*, 2007, **126**, 114503.
14. J.R. Sangoro, A. Serghei, S. Naumov, P. Galvosas, J. Kärger, C. Wespe, F. Bordusa and F. Kremer, *Phys. Rev. E*, 2008, **77**, 051202.
15. C. Iacob, J.R. Sangoro, A. Serghei, S. Naumov, Y. Korth, J. Kärger, C. Friedrich and F. Kremer, *J. Chem. Phys.*, 2008, **129**, 234511.
16. C. Krause, J.R. Sangoro, C. Iacob and F. Kremer, *J. Phys. Chem. B*, 2010, **114**, 382.
17. C. Gainaru, E.W. Stacy, V. Bocharova, M. Gobet, A.P. Holt, T. Saito, S. Greenbaum and A.P. Sokolov, *J. Phys. Chem. B*, 2016, **120**, 11074.
18. E. Thoms, P. Sippel, D. Reuter, M. Weiss, A. Loidl and S. Krohns, *Sci. Rep.*, 2017, **7**, 7463.
19. P. Sippel, S. Krohns, D. Reuter, P. Lunkenheimer and A. Loidl, *Phys. Rev. E*, 2018, **98**, 052605.
20. P.J. Griffin, A.P. Holt, K. Tsunashima, J.R. Sangoro, F. Kremer and A.P. Sokolov, *J. Chem. Phys.*, 2015, **142**, 084501.
21. Y. Yoshimura, H. Abe, Y. Imai, T. Takekiyo and N. Hamaya, *J. Phys. Chem. B*, 2013, **117**, 3264.
22. S. Bista, E. I. Morin and J.F. Stebbins, *J. Chem. Phys.*, 2016, **144**, 044502.
23. I.V. Danilov, E.L. Gromnitskaya and V. V. Brazhkin, *J. Phys. Chem. B*, 2016, **120**, 7593.
24. S. Kapoor, L. Wondraczek and M.M. Smedskjaer, *Front. Mater*., 2017, **4**, 1.
25. C. Calahoo and L. Wondraczek, *J. Non-Cryst. Solids: X*, 2020, **8**, 100054.
26. H. Behrens, *Chemical Geology*, 1992, **96**, 267.
27. F. Gaillard, *Earth Planet. Sci. Lett.*, 2004, **218**, 215.
28. M. Laumonier, F. Gaillard and D. Sifre, *Chemical Geology*, 2015, **418**, 66.
29. T. Yoshino, B. Zhang, B. Rhymer, C. Zhao and H. Fei, *J. Geophys. Res. Solid Earth*, 2017, **122**, 158.
30. M.D. Ingram, B. Macmillan, A.J. Pappin, B. Roling and J.M. Hutchinson, *Solid State Ionics*, 1998, **105**, 103.
31. P.W.S.K. Bandaranayake, C.T. Imrie and M.D. Ingram, *Phys. Chem. Chem. Phys.*, 2002, **4**, 3209.
32. J.L. Souquet, F. Alloin, O. Brylev, M. Duclot and J.Y. Sanchez, *Ionics*, 1998, **4**, 1.
33. C.T. Moynihan, N. Balitactac, L. Boone and T.A. Litovitz, *J. Chem. Phys.*,1971, **55**, 3013.
34. M. Tatsumisago, C.A. Angell and S.W. Martin, *J. Chem. Phys.*, 1992, **97**, 6968.
35. M. Frey, H. Didzoleit, C. Gainaru and R. Böhmer, *J. Phys. Chem. B*, 2013, **117**, 12164.
36. N. Ito and R. Richert, *J. Phys. Chem. B*, 2007, **111**, 5016.
37. P. Griffin, A. L. Agapov, A. Kisliuk, X.-G. Sun, S. Dai, V.N. Novikov and A.P. Sokolov, *J. Chem. Phys.*, 2011, **135**, 114509.
38. P. Griffin, A. L. Agapov and A.P. Sokolov, *Phys. Rev. E*, 2012, **86**, 021508.
39. C. A. Angell, *Solid States Ionics*, 1983, **9**&**10**, 3.
40. W. Xu, E. I. Cooper and C.A. Angell, *J. Phys. Chem. B*, 2003, **107**, 6170.
41. F. Mizuno, J.-P. Belieres, N. Kuwata, A. Pradel, M. Ribes and C.A. Angell, *J. Non-Cryst. Solids*, 2006, **352**, 5147.
42. C.A. Angell, K.L. Ngai, G.B. McKenna, P.F. McMillan and S.W. Martin, *J. Appl. Phys.*, 2000, **88**, 3113.
43. A.L. Agapov and A.P. Sokolov, *Macromolecules*, 2011, **44**, 4410.
44. J.R. Sangoro, C. Iacob, A.L. Agapov, Y. Wang, S. Berdzinski, H. Rexhausen, V. Strehmel, C. Friedrich, A.P. Sokolov and F. Kremer, *Soft Matter*, 2014, **10**, 3536.
45. Z. Wojnarowska, Y. Wang, K.J. Paluch, A.P. Sokolov and M. Paluch, *Phys. Chem. Chem. Phys.*, 2014, **16**, 9123.
46. V. Molinero and W.A. Goddard III, *Phys. Rev. Lett.*, 2005, **95**, 045701.

47. J.R. Sangoro, M. Mierzwa, C. Iacob, M. Paluch and F. Kremer, *RSC Adv.*, 2012, **2**, 5047.
48. K. R. Harris and M. Kanakubo, *Faraday Discuss.*, 2012, **154**, 425.
49. Z. Wojnarowska, J. Knapik, J. Jacquemin, S. Berdzinski, V. Strehmel, J.R. Sangoro and M. Paluch, *Macromolecules*, 2015, **48**, 8660.
50. Z. Wojnarowska, Y. Wang, J. Pionteck, K. Grzybowska, A.P. Sokolov and M. Paluch, *Phys. Rev. Lett.*, 2013, **111**, 225703.
51. Z. Wojnarowska, L. Tajber and M. Paluch, *J. Phys. Chem. B*, 2019, **123**, 1156.
52. I. Chang and H. Sillescu, *J. Phys. Chem. B*, 1997, **101**, 8794.
53. M.V. Kondrin, E.L. Gromnitskaya, A.A. Pronin, A.G. Lyapin, V.V. Brazhkin and A.A. Volkov, *J. Chem. Phys.*, 2012, **137**, 084502.
54. M. Ue, *J. Electrochem. Soc.*, 1994, **141**, 3336.
55. K. Niss and T. Hecksher, *J. Chem. Phys.* 2018, **149**, 230901.
56. J. Kawamura and M. Shimoji, *J. Non-Cryst. Solids*, 1986, **88**, 281.
57. A. Dutta and A. Ghosh, *J. Chem. Phys.*, 2007, **127**, 144504.
58. M. Bonetti, *J. Phys. Chem. B*, 2016, **120**, 4319.
59. M. Bonetti and A. Dubois, *Eur. Phys. J. E*, 2019, **42**, 97.
60. A. Jayaraman, *Rev. Mod. Phys.*, 1983, **55**, 65.
61. R. Letoullec, J.P. Pinceaux and P. Loubeyre, *High Pressure Res.*, 1988, **1**, 77.
62. J. Thomasson, Y. Dumont, J.-C. Griveau and C. Ayache, *Rev. Sci. Instrum.*, 1997, **68**, 1514.
63. R. Jaramillo, Y. Feng and T.F. Rosenbaum, *Rev. Sci. Instrum.*, 2012, **83**, 103902.
64. J. Zabaleta, S.C. Parks, B. Baum, A. Teker, K. Syassen and J. Mannhart, *Rev. Sci. Instrum.*, 2017, **88**, 033901.
65. G.J. Piermarini, S. Block and J.D. Barnett, *J. Appl. Phys.*, 1973, **44**, 5377.
66. H. Jin, G. A. Baker, S. Arzhantsev, J. Dong and M. Maroncelli, *J. Phys. Chem. B*, 2007, **111**, 7291.
67. L.-M. Wang, C.A. Angell and R. Richert, *J. Chem. Phys.*, 2006, **125**, 074505.
68. A. Kudlik, S. Benkhof, T. Blochowicz, C. Tschirwitz and E. Rössler, *J. Molecular Structure*, 1999, **479**, 201.
69. J. Barthel, H.-J. Gores, P. Carlier, F. Feuerlein and M. Utz, *Ber. Bunsenges. Phys. Chem.*, 1983, **87**, 436.
70. J. Barthel and F. Feuerlein, *J. Solution Chem.*, 1984, **13**, 393.
71. T.C. Ransom and W.F. Oliver, *Phys. Rev. Lett.*, 2017, **119**, 025702.
72. Y. Yoshimura, M. Shigemi, M. Takaku, M. Yamamura, T. Takekiyo, H. Abe, N. Hamaya, D. Wakabayashi, K. Nishida, N. Funamori, T. Sato and T. Kikegawa, *J. Phys. Chem. B*, 2015, **119**, 8146.
73. D.L. Sidebottom, B. Roling and K. Funke, *Phys. Rev. B*, 2000, **63**, 024301.
74. F.S. Howell, R.A. Bose, P.B. Macedo and C.T. Moynihan, *J. Phys. Chem.*, 1974, **78**, 639.
75. I.M. Hodge, K.L. Ngai and C.T. Moynihan, *J. Non-Cryst. Solids*, 2005, **351**, 104.
76. A.S. Nowick, A.V. Vaysleyb and I. Kuskovsky, *Phys. Rev. B*, 1998, **58**, 8398.
77. A.S. Nowick and B.S. Lim, *Phys. Rev. B*, 2001, **63**, 184115.
78. F. Bordi, C. Cametti and R. H. Colby, *J. Phys.: Condens. Matter*, 2004, **16**, R1423.
79. M.H. Martin and A. Lasia, *Electrochim. Acta*, 2011, **56**, 8058.
80. P.B. Ishai, M.S. Talary, A. Caduff, E. Levy and Y. Feldman, *Meas. Sci. Technol.*, 2013, **24**, 102001.
81. A.K. Jonscher, *J. Materials Sci.*, 1981, **16**, 2037.
82. D.P.Almond and A.R. West, *Solid State Ionics*, 1983, **11**, 57.
83. J.R. Macdonald, *Solid State Ionics*, 2000, **133**, 79.
84. A. Serghei, M. Tress, J.R. Sangoro and F. Kremer, *Phys. Rev. B*, 2009, **80**, 184301.
85. P. Lunkenheimer, V. Bobnar, A.V. Pronin, A.I. Ritus, A.A. Volkov and A. Loidl, *Phys. Rev. B*, 2002, **66**, 052105.
86. S. Emmert, M. Wolf, R. Gulich, S. Krohns, S. Kastner, P. Lunkenheimer and A. Loidl, *Eur. Phys. J. B*, 2011, **83**, 157.
87. D.L. Sidebottom, *Phys. Rev. Lett.*, 1999, **82**, 3653.
88. D.P. Almond, C.C. Hunter and A.R. West, *J. Materials Sci.*, 1984, **19**, 3236.
89. G.P. Johari and E. Whalley, *Faraday Symp. Chem. Soc.*, 1972, **6**, 23.
90. R. Casalini and S. Bair, *J. Chem. Phys.*, 2008, **128**, 084511.
91. W. Xu, E. I. Cooper and C.A. Angell, *J. Phys. Chem. B*, 2003, **107**, 6170.
92. D.R. MacFarlane, M. Forsyth, E.I. Izgorodina, A.P. Abbott, G. Annata and K. Frasera, *Phys. Chem. Chem. Phys.*, 2009, **11**, 4962.
93. H. Namikawa, *J. Non-Cryst. Solids*, 1975, **18**, 173.
94. J.C. Dyre and T.B. Schroder, *Rev. Mod. Phys*, 2000, **72**, 873.
95. D.L. Sidebottom and J. Zhang, *Phys. Rev. B*, 2000, **62**, 5503.
96. S. Murugavel and B. Roling, *Phys. Rev. Lett*., 2002, **89**, 195902.

97. T.B. Schroeder and J.C. Dyre, *Phys. Rev. Lett.*, 2000, **84**, 310.
98. P. Singh, B.P. Singh and Raghvendra, *Solid State Ionics*, 2012, **227**, 39.
99. E.R. Lopez, A.S. Pensado, M.J.P. Comunas, A.A.H. Padua, J. Fernandez and K. R. Harris, *J. Chem. Phys.*, 2011, **134**, 144507.
100. C. Dreyfus, A. Le Grand, J. Gapinski, W. Steffen and A. Patkowski, *Eur. Phys. J. B*, 2004, **42**, 309.
101. K. Koperwas, A. Grzybowski, K. Grzybowska, Z. Wojnarowska, J. Pionteck, A. P. Sokolov and M. Paluch, , *Phys. Rev. E*, 2012, **86**, 041502.
102. R. Casalini, S.S. Bair and C.M. Roland, *J. Chem. Phys.*, 2016, **145**, 064502.
103. C.M. Roland, S. Bair and R. Casalini, *J. Chem. Phys.*, 2006, **125**, 124508.
104. M.C.C. Ribeiro, A.A.H. Padua and M. F. Costa Gomes, *J. Chem. Phys.*, 2014, **140**, 244514.
105. D. Fragiadakis and C.M. Roland, *Phys. Rev. E*, 2011, **83**, 031504.
106. T.S. Ingebrigtsen, L. Boehling, T.B. Schroeder and J.C. Dyre, *J. Chem. Phys.*, 2012, **136**, 061102.
107. R. Casalini and T.C. Ransom, *J. Chem. Phys.*, 2019, **151**, 194504.
108. S. Pawlus, R. Casalini, C.M. Roland, M. Paluch, S. J. Rzoska and J. Ziolo, *Phys. Rev. E*, 2004, **70**, 061501.
109. R. Casalini, U. Mohanty and C.M. Roland, *J. Chem. Phys.*, 2006, **125**, 014505.
110. R. Casalini and C.M. Roland, *J. Chem. Phys.*, 2018, **148**, 134506.
111. R. Casalini and C.M. Roland, *Macromolecules*, 2013, **46**, 6364.
112. M.D. Ingram, M.A. Mackenzie, W. Müller and M. Torge, *Solid State Ionics*, 1988, **28-30**, 677.
113. P. Jund, W. Kob and R. Jullien, *Phys. Rev. B.*, 2001, **64**, 134303.
114. A.W. Imre, H. Staesche, S. Voss, M.D. Ingram, K. Funke and H. Mehrer, *J. Phys. Chem. B*, 2007, **111**, 5301.